Soft Matter

ARTICLE TYPE

Cite this: DOI: 10.1039/xxxxxxxxxx

Electroosmosis near surfactant laden liquid-air interfaces: Electronic Supplementary Information†

Baptiste Blanc[a], Oriane Bonhomme[a], Pierre-Francois Brevet[a], Emmanuel Benichou[a], Christophe Ybert[a] and Anne-Laure Biance*[a]

Received Date
Accepted Date

DOI: 10.1039/xxxxxxxxxx

www.rsc.org/journalname

1 Experimental procedures

1.1 Chemical and cleaning procedures

Tetradecyltrimethylammonium bromide (TTAB, with a critical micellar concentration cmc $= 4.5\ 10^{-3}$ mol/L[1]) is purchased from *Sigma Aldrich* and used as received. Surfactants are added to deionized water (*millipore*) at a concentration c varying from 4.5 μmol/L to 13.5 mmol/L. Solutions are renewed every day to avoid aging phenomena. The bulk conductivity of the solutions is systematically measured with an electrical conductivity meter (EC meter, *Hanna Instrument*). Fluorescent polystyrene spheres of diameter 200 nm (amine-modified microspheres, yellow-green fluorescent (505/515nm), 2 % solids by *Invitrogen*) are added in the solution at a volume ratio of 1/1000. Zeta potential of these particles ζ_P are measured in each surfactant solution with a commercial zetameter (Zetasizer NanoZS 90, *Malvern Instruments*, Fig.3). The cell is made of PDMS (polydimethylsiloxane) mixed with a reticulating agent and deposited around a parallellepipedic mold of surface size 1 cm x 1 cm or 4 cm x 4 cm (depending on the size of the cell used) in a petri dish. It is then placed in an oven at 80^{o}C during at least one hour for reticulation. After mold removing, a glass plate cleaned in a plasma cleaner apparatus is stuck to the bottom surface of the cell. The upper side is open. Before pouring the specified solution, the cell is washed three times with deionized water, ethanol, and then deionized water again. The cell is filled with the solution with a level higher than 3.7 mm to avoid contributions from electro-osmotic (EO) flows generated at the bottom glass plate (for more details, see section *ζ-potential measurement*). Ag/AgCl electrodes are made from silver sheets (thickness 125 μm or 250 μm, *GoodFellow*), resting at least 48 hours in a highly concentrated bleached solution to create the AgCl layer. They are then rinsed with deionized water thoroughly.

1.2 Applied electric field

As classically done (*e.g.* in commercial zetameters), AC electric fields have been used to to be able to filter constant drift phenomena, and to minimize electrode issues[2]. For instance, water electrolysis creates hydrogen and oxygen bubbles, but also releases protons and hydroxide ions that can alter the local pH, local potential and ion mobility. Applying an AC electric field avoids these drawbacks[3,4]. The AC electric field is created through an AC generator with voltage ranging from 0 to 30V peak-to-peak. Unless specified, the driving frequency is set to 2 Hz throughout the present study.

To assess the goodness of electrodes, and the absence of aging of the system due to electrode deterioration or solution evolution (because of electrochemical reactions), different tests are performed. First the pH has been measured and is shown to remain constant at a value of 5.5 before and after the experiment, in agreement with water at equilibrium with atmospheric CO_2. Moreover, the electrical current in the system is constantly monitored. Knowing the trough geometry, the solution conductivity is then deduced and compared to its independent benchmark value obtained with the same fresh solution in the commercial conductivity meter. Values obtained in our experimental cell, with the Ag/AgCl electrodes, agreed with the reference measurement. Fig. 1a shows the evolution of the in-situ conductivity as a function of the surfactant concentration. The theoretical conductivity and its c linear dependency is well recovered with a saturation arising below 50 μmol/L, due to proton conductivity (pH=5.5), which is expected to be dominant at concentrations lower than 1.2x10^{-5}mol/L, i.e. 2.5x10^{-2}cmc. Note that at the lowest concentrations, some scattering develops as a signature of difficulties to fully control the physical and chemical characteristics of the system. This accuracy of the current is used as a check for validating the experimental procedure.

Moreover, over the course of an experiment, no evolution of the conductivity beyond 5% was recorded, showing that the system is indeed stable with no significant evolution of the electrode

---

[a] *Univ Lyon, Université Claude Bernard Lyon 1, CNRS, Institut Lumière Matière, F-69622, VILLEURBANNE, France; E-mail: anne-laure.biance@univ-lyon1.fr*

properties or of the solution composition. Furthermore no phase shift between the applied tension and the measured electrical current has been observed, ruling out some electrode polarization effects.

Finally, we also checked for another but similar system (SDS surfactants, anionic, and carboxylate modified polystyren beads as also negatively charged fluorescent probes, other parameters remaining similar) that the electrode response is linear, and that the voltage applied in this range (limited due to acquisition constraints) has no influence on the experimental results of the *zeta*-potential. These specific tests are reported in Fig. 1b.

1.3 Bead displacement acquisition

An inverted confocal microscope (*Leica* TCS SP5 DMI6000) is used to follow the displacement of the bead in the liquid. The fluorescent probes are imaged by a 10× objective with a numerical aperture NA of 0.3 (HC Plan *Fluotar Leica*) leading to a theoretical depth of field of $\Delta z = \frac{2n\lambda_L}{NA^2} = 16\ \mu$m. Determination of the optical system characteristics has been performed by investigating the intensity of the laser reflexion on the liquid gas interface for different altitude. In our configuration, the objective point spread function ranges up to 70 μm. 256×1024 pixel images are recorded at a frame rate of 1 every 39 ms to achieve a sampling of above 10 images per voltage periods. For each depth, a stack of 100 images is acquired spanning 8 driving periods. The air-liquid interface is localized using reflected light signal of the laser beam. From there the vertical sampling is organized as follows: one measurement every 26 μm over the first 400 μm followed by one measurement every 133 μm up to $z = 2000\,\mu$m.

Analysis of the image stacks is done through image correlation techniques[5] to yield the average displacement of particles at a given z, as a function of time. Hundreds of colloids contribute to the images thus ensuring excellent statistics. Moreover, Brownian diffusion is slow enough to prevent particles leaving the observation volume over the course of the recording. Indeed, with $D = 2\,\mu\mathrm{m}^2/\mathrm{s}$, particles diffuse up to only 2 μm over a driving period, and up to only 5.6 μm over the full stack recording. This is to be compared with the typical bead excursion due to the oscillating field (typically around 10 μm) and to the theoretical depth of the image stack (around 16 μm) confirming our ability for an accurate extraction of the convective bead motion. Moreover, note that in term of image correlation, the statistical displacement of a colloid assembly due to diffusion is zero so that such random displacement results in a broadening of the correlation peak but not in net translation. Therefore the bead convective motion is perfectly recovered.

In Fig. 2 are displayed the raw displacement data extracted from the previous protocol. As can be seen, a constant drift is generically superimposed to the field-driven oscillating behavior, and is indeed a classical reason for using AC drivings in *zeta*-potential measurements. Indeed, in the framework of linear response theory, the whole electro-osmotic —and thus *zeta*-potential— information is fully contained in the oscillatory component displacement. Note that the validity of linear response was verified by varying the voltage driving amplitude as shown in Fig. 1. Raw displacement were thus filtered at the driving frequency to extract the linear response component alone. The 8-period long oscillating displacement is fitted with a sinusoidal function to extract the displacement amplitude $A(z)$ which is shown and analyzed in inset of Fig. 2 of the main text, or in Fig 1b.

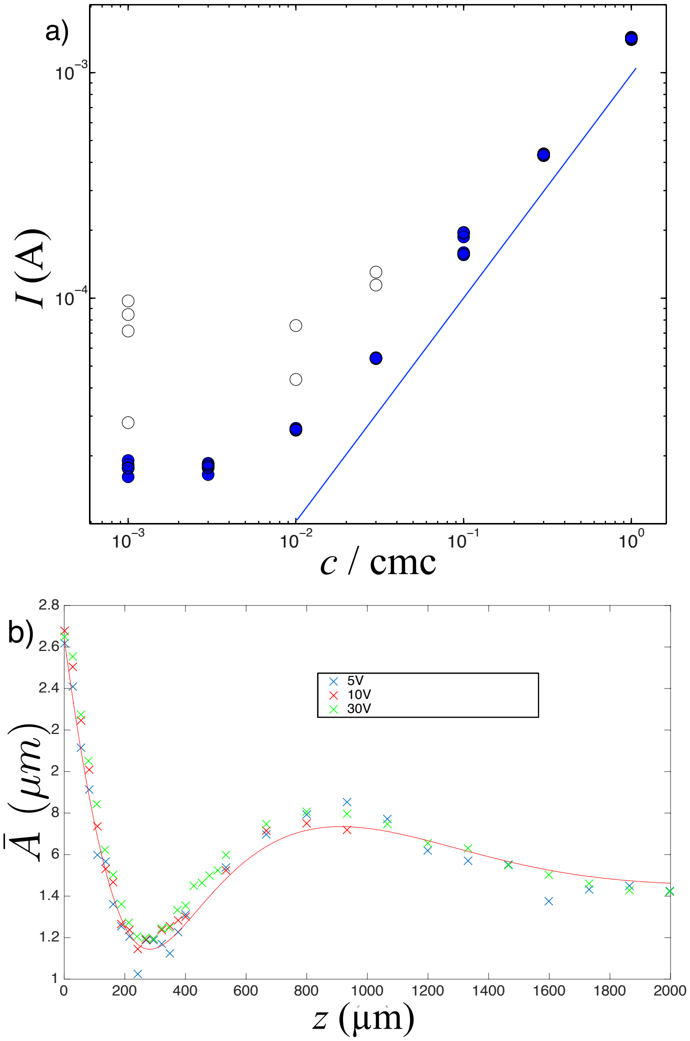

Fig. 1 a) Measured current when 10V is applied in the tank varying TTAB concentration. The plain line corresponds to the theoretical expected current in the high concentration limit, knowing our cell geometry and TTAB concentration. The open symbols correspond to data points which are not considered in the experiments (they do not satisfy our check-list). At low concentration, proton conductivity is not negligible and a saturation is observed. The linearity is recovered at large concentration showing that the electrode conversion efficiency is good. b) Amplitude of bead displacement $\bar{A}$ normalized by the applied voltage ($\bar{A} = A$*10/ΔV) versus the distance from the interface z for a 0.07 mM SDS solution (Sodium Dodecyl Sulfate, *Sigma Aldrich*). The three profiles acquired for three different applied voltages satisfactorily superimposed, showing the linearity of the EO response. The plain line corresponds to a fit following eq.(1). In this case of anionic surfactants, negatively charged fluorescent beads (carboxylate modified, *Invitrogen*, 200nm) are employed.

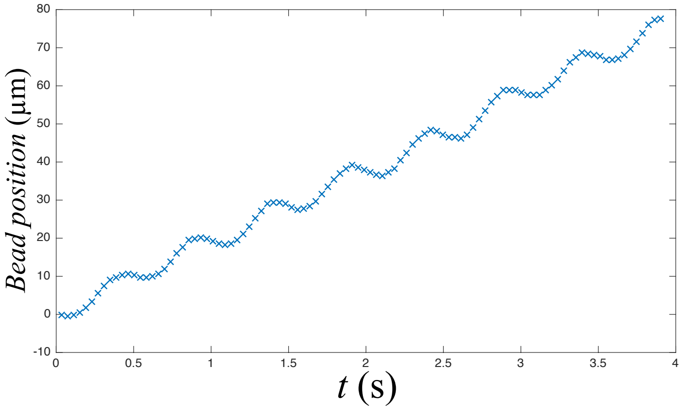

Fig. 2 Measurement of bead positions versus time (imposed frequency is 2Hz, z=160 μm, c=0.03cmc.)

1.4 ζ-potential measurement: phase shift and bead electrophoretic velocity

As already stated, a great care was taken to ensure reproducibility by tracking possible time evolution of the system resulting from defective electrodes. In addition to the validation elements brought by the recording of the electric current and solution conductivity, the z-profiles of the bead displacement were systematically recorded in a back-and-forth protocol. This protocol allowed to detect any hysteresis in the obtained values of the displacements: all experiments that did not fulfill the requirement of identical back-and-forth profiles were discarded from the study.

Each experimental profile is then fitted using equation (1)

$$A(z) = \frac{U_i}{\omega}\sqrt{e^{-\frac{2z}{z_0}} - 2\frac{U_P}{U_i}e^{-\frac{z}{z_0}}\cos(\frac{z}{z_0}-\phi_P)+\frac{U_P^2}{U_i^2}} \quad (1)$$

with U_i, U_P and ϕ_P as free parameters. Concerning z_0, the typical length of viscous momentum diffusion ($z_0 = \sqrt{\frac{2\eta}{\rho\omega}}$), it is entirely fixed by the driving frequency and by the liquid bulk properties. For the 2 Hz driving, the fixed value of $z_0 = 416\,\mu$m is used. Note that this equation corresponds to the superposition of a constant electrophoretic velocity and of an oscillating viscous boundary solution arising from the free surface. Ignoring the similar flow developing at the bottom plate requires to be sufficiently far apart from the measurement location. Considering $z_0 = 416\,\mu$m and the deepest measurement performed at 2000 μm, this is ensured by imposing a total liquid height above 3.7 mm.

Far from the interface, the motion of the particle is only given by its electrophoretic contribution i.e. $U_P = \frac{\zeta_P \varepsilon E}{\eta}$. A consistency check of the results extracted from the experimental fit procedure can be performed by comparing the obtained values for ζ_P with independent results obtained with a commercial ζ-meter (Zetasizer NanoZS 90, *Malvern Instruments*) on similar solution. Such comparison is reported in Fig. 3 and shows a very satisfactory agreement. Some deviations are however observed. This effect might be due to a residual meniscus effect near electrodes which deforms the free surface and affect the field lines. We then used the reference zetameter ζ_P value to deduce from U_P the real applied electric field amplitude associated with the longer electrode-to-electrode curvilinear distance.

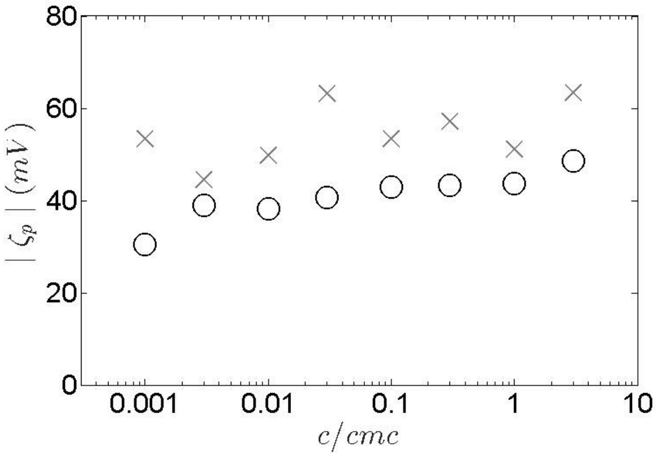

Fig. 3 ζ-potential of particles against the bulk concentration c/cmc measured with the commercial zetameter (black circle) and with our experimental set-up (grey crosses).

Finally, let us mention that in the theoretical expression of the flow profile eq.(1), a phase shift has been introduced between the electrophoretic and electro-osmotic component. This phase shift ϕ_P is rather constant over the different experimental conditions as shown in Fig. 4, with typical value $\phi_P \sim 0.15 \pm 0.1$. Such a small but finite phase shift is indeed expected as soon as any averaging process or systematic error in the z location will affect only the electro-osmotic phase. In practice error bar in the free surface location, asymmetry in the objective point-spread function and z-averaging over the image depth-of-field all cumulate and contribute to such a finite phase shift. The depth of field of the objective (Δz) gives us an order of magnitude of the total uncertainties and the expected phase shift, around $\Delta z/z_0 \sim 0.17$, in fair agreement with the observations.

The experiments have been repeated several times at each concentration, and results reported of the ζ-potential (fig. 2 of the main text) and the phase shift (Fig. 4) corresponds to averaged values, error bar magnitudes corresponding to standard deviations of the results.

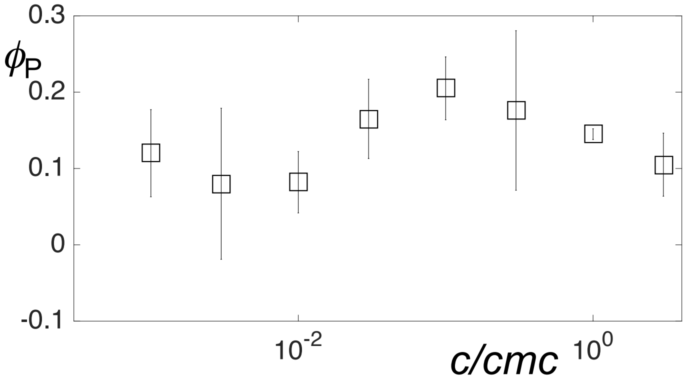

Fig. 4 Phase shift ϕ_P obtained from the fit (eq.1) against the surfactant concentration c/cmc.

2 Surface coverage by SHG measurements

Second Harmonic Generation is a non-linear optical technique commonly used to characterize surfaces. This phenomenon consists in the conversion of two photons at a given frequency $2\pi/\lambda_i$ where λ_i is the laser beam wavelength in a unique photon at the double frequency ($4\pi/\lambda_i$). Due to symmetry properties, this phenomenon is possible only at places where centrosymetry is broken, it is thus a tool of choice to study interfaces and interfacial phenomena. We propose to use this technique to characterize the surface composition of surfactant solutions. We focus here on TTAB solution below and above the cmc.

2.1 Experimental procedure

The SHG experiment is already described in literature[6]. The experiments are performed with a Ti-Sa femtosecond oscillator with a pulse-duration around 70 fs, repetition rate of 80 MHz (*Spectra Physics*, model Tsunami). Its power at the fundamental wavelength $\lambda_i = 810$ nm is approximately 1 W at the output. The laser is filtered to remove any unwanted wavelength, linearly polarized (p- polarization) and focused with a 5 cm focal length lens on the interface under study. The incident angle is $70 \pm 5^\circ$ compared to the surface normal to optimize the SHG intensity and the typical beam diameter on the interface is 100 μm. We collect the reflected beam with a 10 cm lens. We study here only the reflected p-polarized harmonic blue light (at 405 nm, the SHG signal) by filtering out the fundamental beam. We acquire the spectrum of the processed beam with a spectrometer and a cooled CCD camera and record the peak intensity value (I_{SHG}).

Before any experiment on TTAB solution, we perform a reference experiment on water: the SHG intensity of a bare water/air interface ($I_{SHG,water}$) is used to normalize all other measurements (necessary to avoid side effects due to fluctuations in the laser power or in the experiment alignment). When we put the solution in the tank in order to create the bath, we adjust the tank position to be perfectly focused and measure the signal intensity without any time delay. We perform 3 to 8 experiments (with different fresh interfaces) at each concentration and error bars correspond to the relative dispersion of the measurements. Due to geometrical constraints (meniscus near the tank border and angle of incidence of the laser beam), most of the spatial investigation with SHG experiments have been performed in a tank (4 cm×4 cm) larger than the device used for ζ-potential determination. This allows a more accurate scanning versus the x position of the signal. Effect of tank size has however been checked, by comparing results in the 1 cm×1 cm and 4 cm×4 cm tank as reported in Fig. 5 and Fig.6. Similarly to observations on the large tank (see main text), no notable lateral variation of the surfactant density on the smaller tank has been observed.

2.2 Analysis of the SHG intensity

Here, we use non-resonant molecules so we can assume that the SHG signal is due to all species at the interface independently. We thus can write:

$$I_{SHG} \sim |\sum_i N_i < \beta_i > |^2 \tag{2}$$

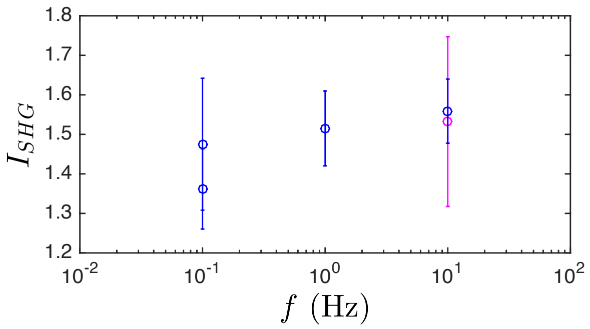

Fig. 5 SHG reflected intensity versus imposed voltage frequency for 0.02 cmc in a small tank (1cm x 1cm). Laser spot is focused 4 mm away from the electrodes (blue) and 3 mm away (pink).

where i refers to all species (here water and TTAB), N_i the number of considered species, β_i the hyperpolarisability tensor of the i-th species (its non-linear optic cross section at the molecular scale) and $< \cdot >$ the average orientation tensor of these species. In our case, this equation simplifies[7]:

$$I_{SHG} = |N_s < \beta_s > + N_w < \beta_w > \exp i\Phi|^2 \tag{3}$$

where the s-index points to surfactant molecules and the w-one the water ones. We add an unknown phase delay (Φ) in this equation to have a general expression, but it is not investigated here. The hyperpolarisabilty tensor of TTAB is unchanged with TTAB concentration as the water term. Literature also proved that the average orientation of the TTAB molecules is unchanged when the bulk concentration is increased[8]. Consequently, in previous equation, all terms are constant except N_s – which is the surface coverage, namely Γ in the following – which evolves. We then plot $\sqrt{I_{SHG}}$, normalized by $\sqrt{I_{SHG,water}}$ as a function of the bulk surfactant concentration in Fig.3 of the main text to test if it is indeed correlated to surface coverage Γ and observed a good agreement at small concentration (below 0.1 cmc), *i.e.* when surfactant molecules adsorbed at the interface are independent of one another. At concentration higher than 0.2 cmc, we note a deviation between the optical measurement and the surface coverage deduced from Gibbs isotherm and Langmuir law. Indeed, looking at SHG theory in more details[9], one can conclude that other factors can contribute to $\sqrt{I_{SHG}}$, such as a constant orientation of water molecules just under the surface due to the electrostatic potential in the Debye layer (as also shown recently[10]). If we take both contributions into account, one would indeed expect a maximum when both contributions are similar, near cmc/5.

3 Motion of surfactants and hydrodynamic boundary condition

3.1 Surfactant exchange rate and effect of applied voltage frequency

We discuss here the possibility of surface-bulk exchange dynamics to cancel out the building of surface-concentration gradients, hence being an alternative explanation to the absence of inhomogeneity in the SHG signal. The characteristic timescale for exchanges is given for diffusion-limited transport[11] by $\tau = 2/D(\partial\Gamma/\partial c)^2$

with $D \simeq 3.2\,10^{-10}$ m^2/s [12]. With the variations of Γ with concentration given by fitted Langmuir isotherm, one deduces a typical exchange rate characterized by $\tau \simeq 250$ ms. This is indeed close to the imposed timescale (500 ms at 2 Hz) meaning that it might affect the amplitude of possible surface concentration gradients, but would not be able to cancel them out. To confirm that surface-bulk exchange is indeed not responsible for the absence of surface gradients, SHG experiments for different frequencies of the applied voltage (up to 100 Hz i.e. beyond the characteristic timescale of exchange) have been carried out and one can observe that the SHG signal is constant whatever the applied frequency (Fig. 6).

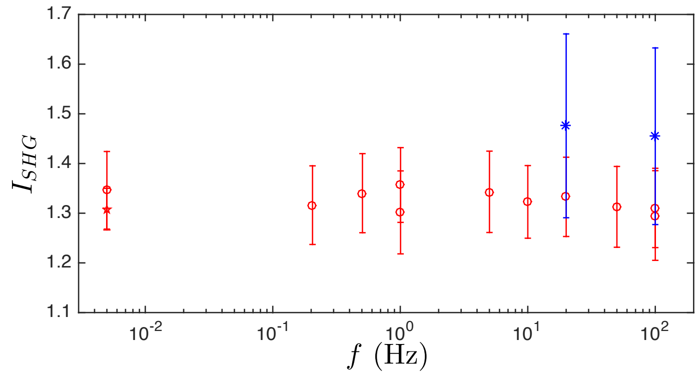

Fig. 6 Normalized SHG signal versus applied voltage frequency for an experiment performed with an 8 V applied voltage in a 4x4 cm tank versus time for a bulk TTAB concentration of 0.019 cmc. o-Acquisition time: 0.02s, *-Acquisition time: 0.005s. In both cases, the signal has been recorded 5mm away from the tank border.

3.2 Momentum balance on the surfactant layer

In a steady state, the surfactant layer would experience different forces as detailed below. The first one corresponds to the electric stress due to the external electric field. This stress reads $\sigma_e = \theta\Gamma eE$ where θ is the non-binded surfactant fraction. Secondly, the surfactants are also submitted to the viscous drag from the water subphase. This friction reads $\sigma_f = \eta \partial v_l / \partial z\,|_{z=0}$ with v_l the liquid velocity. Integrating the Stokes equation in the liquid $\eta \partial v^2 / \partial z^2 = (c_+ - c_-)eE$, one recovers

$$\eta \left(\frac{\partial v_l}{\partial z}\,|_{+\infty} - \frac{\partial v_l}{\partial z}\,|_0 \right) = \int_0^{+\infty} (c_+ - c_-)eEdz \qquad (4)$$

which reduces in

$$-\eta \frac{\partial v_l}{\partial z}\,|_0 = \theta e \Gamma E \qquad (5)$$

Canceling out both contributions simply arises from the global neutrality of the system {adsorbed surfactant + underneath solution} which imposes no net force on the system. Assuming a relative motion of the surfactant layer with respect to the air would lead to a non-zero additional friction force which is incompatible at steady-state with the absence of net driving force.

Hence after a transient regime during which momentum can be exchanged with the outside to generate friction in the liquid system, no net motion of the surfactants with respect to the surrounding air can persist, thus indicating an immobile layer in the laboratory reference frame. To determine if the quasi-steady state hypothesis sustains, one should compare the timescale of velocity variations in the experiments with the transient one (see main text). Note that similar reasoning for force balance close to interfaces was already discussed in the vicinity of neutral hydrophobic surfaces [13].

3.3 Expected effect of slippage

Now that we demonstrate that surfactants are immobile, we can estimate if in our experimental conditions, slippage is relevant to be observed. In this case, one would expect that the observed ζ-potential is enhanced compared to static surface potential by a factor $1 + bV'(z=0)/V(z=0)$ [14], which reduces to $1 + b/\lambda$ at low surface and consequently concentration, b being the slip length [15] and λ the Debye length defined as $\lambda = \sqrt{\varepsilon kT/2e^2c}$. Following numerical predictions [16], the slip length of water on surfactant heads is expected to vary with the surfactant surface concentration as $b = 1/(3\pi R\Gamma)$, with R the size of the surfactant head we estimate to be 0.5 nm. Varying surfactant bulk concentration, and using Langmuir isotherm to obtain $\Gamma(c)$, the values of λ and b can be calculated and we can plot in our experimental conditions the ratio between them (Fig. 7) versus bulk concentration. We see that potential enhancement due to slippage remains limited to 20 % in our range of concentration.

We can then try to estimate the value of the ζ potential in the limit of vanishing surface charge. In our experimental conditions, complexity arises for example due to surfactant partial dissociation, as mentioned above. In the literature, it has been shown that this dissociation, even though saturating at large surface charge density (as reported here), tends to increase when Γ decreases, reaching one in the limit of zero surface charge. We can then assume that, at first order, in the limit of low c, each surfactant head bears one charge [16]. Then, we can use linearized Poisson Boltzmann framework to estimate the surface potential ($V_s = e\Gamma\lambda/\varepsilon$) and we then expect a saturation of the ζ-potential of $\zeta_{sat} = e/3\pi\varepsilon R =$ 50 mV, surprisingly in good agreement with our experimental results at low c [1,16–21].

References

1 V. Bergeron, *Langmuir*, 1997, **13**, 3474–3482.
2 Y. Fukui, S. Yuu and K. Ushiki, *Powder technology*, 1988, **54**, 165–174.
3 M. Oddy and J. Santiago, *Journal of colloid and interface science*, 2004, **269**, 192–204.
4 M. Mayur, S. Amiroudine, D. Lasseux and S. Chakraborty, *Electrophoresis*, 2014, **35(5)**, 670–680.
5 B. Hebert, S. Costantino and P. W. Wiseman, *Biophysical journal*, 2005, **88**, 3601–3614.
6 G. Martin-Gassin, E. Benichou, G. Bachelier, I. Russier-Antoine, C. Jonin and P.-F. Brevet, *The Journal of Physical Chemistry C*, 2008, **112**, 12958–12965.
7 Y.-C. Wen, S. Zha, X. Liu, S. Yang, P. Guo, G. Shi, H. Fang, Y. R. Shen and C. Tian, *Phys. Rev. Lett.*, 2016, **116**, 016101.

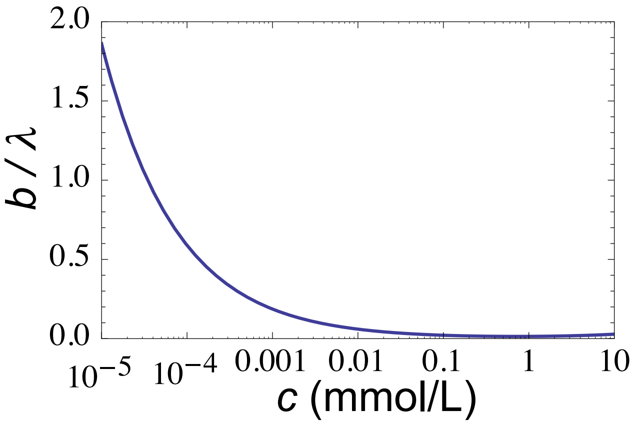

Fig. 7 Expected ζ-potential enhancement, given by the ratio of the expected slip length b and the Debye length λ, as a function of the surfactant bulk concentration c.

8 C. M. Johnson and E. Tyrode, *Physical Chemistry Chemical Physics*, 2005, **7**, 2635–2640.

9 W. Chen, M. B. Feller and Y. R. Shen, *Phys. Rev. Lett.*, 1989, **63**, 2665–2668.

10 K. T. Nguyen, A. V. Nguyen and G. M. Evans, *J. Phys. Chem. C*, 2015, **119**, 15477–15481.

11 D. Langevin, *Annual Review of Fluid Mechanics*, 2014, **46**, 47–65.

12 A. C. Ribeiro, V. M. Lobo, A. J. Valente, E. F. Azevedo, M. d. G. Miguel and H. Burrows, *Colloid and Polymer Science*, 2004, **283**, 277–283.

13 D. M. Huang, C. Cottin-Bizonne, C. Ybert and L. Bocquet, *Phys. Rev. Lett.*, 2007, **98**, 177801.

14 L. Joly, C. Ybert, E. Trizac and L. Bocquet, *Phys. Rev. Lett.*, 2004, **93**, 257805.

15 L. Bocquet and E. Charlaix, *Chemical Society Reviews*, 2010, **39**, 1073–1095.

16 L. Joly, F. Detcheverry and A.-L. Biance, *Phys. Rev. Lett.*, 2014, **113**, 088301.

17 J. Israelachvili, *Intermolecular and Surface Forces, Third Edition*, Academic Press, 2010.

18 V. Kalinin and C. Radke, *Colloids and Surfaces A: Physicochemical and Engineering Aspects*, 1996, **114**, 337–350.

19 C. M. Phan, *J. Phys. Chem. B*, 2016, **120**, 7681–7686.

20 R. Zana, S. Yiv, C. Strazielle and P. Lianos, *Journal of Colloid and Interface Science*, 1981, **80**, 208–223.

21 P. Carpena, J. Aguiar, P. Bernaola-Galván and C. Carnero Ruiz, *Langmuir*, 2002, **18**, 6054–6058.